

Experimental Validation of a Grid-Aware Optimal Control of Hybrid AC/DC Microgrids

Willem Lambrichts*, Jules Macé† and Mario Paolone*

* Distributed Electrical System Laboratory (DESL)

EPFL, Lausanne, Switzerland

† Power Electronics Laboratory (PEL)

EPFL, Lausanne, Switzerland

Abstract—This paper presents the experimental validation of a grid-aware real-time control method for hybrid AC/DC microgrids. The optimal control is leveraged by the voltage sensitivity coefficients (SC) that are computed analytically using the close-form expression proposed in the authors' previous work. The SCs are based on the unified power flow model for hybrid AC/DC grids that accounts for the AC grid, DC grid, and the Interfacing Converters (IC), which can operate in different control modes, e.g. voltage or power control. The SCs are used to express the grid constraints in the optimal control problem in a fully linear way and, therefore, allow for second- to subsecond control actions. The validation of the model is performed on the hybrid AC/DC grid, available at the EPFL. The network consists of 18 AC nodes, 8 DC nodes, and 4 converters to interface the AC and DC network. The network hosts multiple controllable and uncontrollable resources. The SC-based optimal control is validated in a generic experiment. It is shown that the real-time control is able to control the ICs optimally to redirect power through the DC grid, to avoid grid constraint violations while providing reactive power support to the upper layer AC grid. Furthermore, the computational time of the optimal control is analysed to validate its application in critical real-time applications.

Index Terms—Hybrid AC/DC networks, Sensitivity Coefficients, Optimal Control, Experimental Validation

I. INTRODUCTION

Hybrid AC/DC microgrids are a promising solution for future power grids that are relying heavily on renewable sources. In fact, integrating AC and DC networks have several advantages, such as an increased overall efficiency of the system [1], allows for more flexible control (through the presence of controllable AC/DC Interfacing Converters (IC)), and reduces the cost of the system because fewer power conversion sources are required as DC sources and loads are directly connected in the DC grid) [1], [2].

Real-time optimal control strategies are crucial for the operation of such grids to regulate the various Distributed Energy Resources (DER) in an optimal way in order to avoid, e.g., grid constraint violations while achieving a certain

objective, such as minimising losses or maximising self-consumption. Optimal Power Flow (OPF) in hybrid AC/DC networks has been intensively studied in the past, particularly in the application of High-Voltage Direct Current systems [3], [4]. However, for AC/DC networks with multiterminal architectures, the literature has presented less robust solutions for optimal control strategies. In general, the proposed methodologies predominantly rely on three approaches: 1) droop control mechanisms of the IC [1], [5], [6], 2) decomposition of the problem where the AC and DC system are treated individually [7], [8] or 3) relaxation techniques of the non-convex ICs' constraints using second-order cone programming [9], [10].

The nature of the above-mentioned problem formulations generally limits the versatility of the different control modes of ICs and, furthermore, restricts the regulation of the DC voltage to a single IC [11]. Generally, the inner control loops of the IC regulate two variables simultaneously as a result of the decoupling of the d and q frames. Typically, the DC voltage or active power is controlled together with the reactive power. The control modes are referred to as power control: $P_{ac}-Q_{ac}$, or voltage control: $E_{dc}-Q_{ac}$. The existing methods presented in the literature allow only one IC to regulate the DC voltage. Therefore, the flexibility of the hybrid network and the security of supply during, e.g. islanding manoeuvres, are greatly reduced. Indeed, when multiple voltage-controlled ICs are present, the power required to obtain the DC voltage can be shared over multiple ICs. This allows for a broader operation and improves the redundancy of the system in the event of failure. Furthermore, it also allows for different voltage levels within the DC grid, which makes it interesting for resources operating at different voltages [12].

In view of the above, this paper presents an experimental validation of an optimal real-time control algorithm for hybrid AC/DC networks. The optimal control is based on the unified Power Flow (PF) method for hybrid grids presented in [13]. The hybrid model includes the AC grid, DC grid, and ICs, which can operate on different control modes (voltage or power control) and, compared to other works presented in the literature, allows multiple ICs to regulate the DC voltage.

The optimal control is based on the linearisation of the unified power flow model, usually referred to as sensitivity coefficients (SC). These are the partial derivatives of the nodal

The project has received funding from the European Union's Horizon 2020 Research & Innovation Programme under grant agreement No. 957788.

voltages and branch currents with respect to the nodal power injections. The SCs allow to formulate the non-convex voltage and current flow equations as a linear constraint in the optimal control problem.

This work uses the method proposed in [14] to obtain a closed-form expression of the SC allowing an efficient analytical computation. The method is extended for hybrid AC/DC networks in [15] and allows to include the unified grid model as constraints of the optimal control problem while accounting for the different control modes of the IC. The linearised OPF formulation is very well suited for real-time control where the network state is provided by a State Estimation (SE) algorithm at high rates:

- 1) The real-time control requires a convex grid model that can be solved efficiently. The SCs allow to reformulate the non-convex PF model into a linear constraint where the uniqueness of the optimal solution is guaranteed. [14]
- 2) The closed-loop formulation of the SC requires only knowledge of the state of the grid and its admittance matrix. In this paper, the states are estimated multiple times per second with very low latency by the linear SE that simultaneously computes the state of the AC and DC grids [16]. Because two consecutive states are not changing significantly, the linear approximation is valid and allows for a very efficient computation with almost no loss in accuracy.

The SC-based optimal control is experimentally validated on the hybrid AC/DC microgrid developed at the EPFL. The hybrid network consists of 18 AC nodes, 8 DC nodes, and 4 converters that interface the AC and DC systems at different nodes. The four ICs operate in voltage control mode; that is, the DC voltage and the reactive power are regulated. Furthermore, resonant DC/DC converters are present to regulate the power flow in the DC network. Various resources are connected to the AC grid, such as three photovoltaic plants, an electric vehicle charging station (EVCS), and a controllable load that acts as a household.

The structure of the paper is as follows: Section II discusses the analytical computation of the SC and presents the formulation of the optimal control problem. In Section III, the hybrid AC/DC grid and its resources are presented. Section IV presents the results of the experimental validation.

II. METHODOLOGY

A. Hybrid AC/DC network model

Consider a generic hybrid AC/DC network with $i \in \mathcal{N}$ AC nodes and $j \in \mathcal{M}$ DC nodes, where buses $(l, k) \in \Gamma$ are the couples of AC/DC converter buses (see Fig.1). Furthermore, we assume $l \in \mathcal{N}$ and $k \in \mathcal{M}$.

The AC network consists of three types of buses: a slack node (\mathcal{N}_{slack}), PV nodes (\mathcal{N}_{PV}) and PQ nodes (\mathcal{N}_{PQ}), and is modelled using the standard PF theory. The AC network

is described as $\bar{\mathbf{I}}^{ac} = \bar{\mathbf{Y}}^{ac} \bar{\mathbf{E}}^{ac}$, where $\bar{\mathbf{E}}^{ac}$ is the phase-to-ground nodal voltage vector, $\bar{\mathbf{I}}^{ac}$ the nodal current injections and $\bar{\mathbf{Y}}^{ac}$ the compound admittance matrix, which is assumed to be known.

The DC network is modelled identically to the AC network with $Q = 0$ and $\bar{\mathbf{Z}} = R$ to reuse the AC-PF theory. There are two types of nodes in the DC grid: voltage controllable nodes: V nodes (\mathcal{M}_V), and power controllable nodes: P nodes (\mathcal{M}_P). The DC network is described as $\mathbf{I}^{dc} = \mathbf{Y}^{dc} \mathbf{E}^{dc}$, with \mathbf{E}^{dc} the DC voltage and \mathbf{I}^{dc} the DC nodal current injections. \mathbf{Y}^{dc} is the compound admittance matrix of the DC grid.

Therefore, $\mathcal{N} = \mathcal{N}_{slack} \cup \mathcal{N}_{PQ} \cup \mathcal{N}_{PV} \cup \Gamma_l$ and $\mathcal{M} = \mathcal{M}_{Pdc} \cup \mathcal{M}_{Vdc} \cup \Gamma_k$

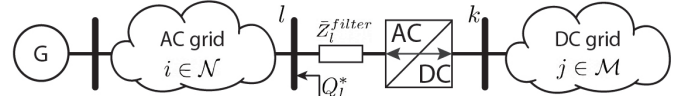


Fig. 1: The generic hybrid AC/DC network. Only one AC/DC converter is displayed for simplicity.

The AC and DC networks are interconnected by one or more ICs (that is, $|\Gamma| \geq 1$) and can operate under different control modes. Because of the nature of the ICs, which are typically Voltage Source Converters (VSC), it is not possible anymore to use the traditional PF theory, and an extension is needed where the model equations are dependent on the converter's operational mode: $E_{dc} - Q_{ac}$ or $P_{ac} - Q_{ac}$ nodes. Tab. I gives an overview of the possible node types in hybrid AC/DC grids. Note that at least one IC or DC source is required to impose the DC voltage (E_{dc}) [17]. The generic and unified power flow model for hybrid AC/DC networks is presented in [13] and used in the experimental validation of the optimal control algorithm in this work.

TABLE I: Different types of nodes in hybrid AC/DC networks and their known and unknown variables.

Bus Type	IC contrl.	Known var.	Unknown var.	Index
AC slack		$ E_{ac} , \angle E_{ac}$	P_{ac}, Q_{ac}	$s \in \mathcal{N}_{slack}$
P_{ac}, Q_{ac}		P_{ac}, Q_{ac}	$ E_{ac} , \angle E_{ac}$	$i \in \mathcal{N}_{PQ}$
$P_{ac}, E_{ac} $		$P_{ac}, E_{ac} $	$Q_{ac}, \angle E_{ac}$	$i \in \mathcal{N}_{PV}$
IC_{ac}	$\frac{P_{ac} - Q_{ac}}{E_{dc} - Q_{ac}}$	$\frac{P_{ac} Q_{ac}}{Q_{ac}}$	$\frac{ E_{ac} , \angle E_{ac}}{P_{ac} E_{ac} \angle E_{ac}}$	$l \in \Gamma_{PQ}$ $l \in \Gamma_{E_{dc}Q}$
IC_{dc}	$\frac{P_{ac} - Q_{ac}}{E_{dc} - Q_{ac}}$	$\frac{P_{dc}}{E_{dc}}$	$\frac{E_{dc}}{P_{dc}}$	$k \in \Gamma_{PQ}$ $k \in \Gamma_{E_{dc}Q}$
P_{dc}		P_{dc}	E_{dc}	$j \in \mathcal{M}_P$
E_{dc}		E_{dc}	P_{dc}	$j \in \mathcal{M}_V$

B. Analytical computation of the sensitivity coefficients

The PF equations of hybrid AC/DC networks are strongly non-linear [13]. As discussed in Section I, the PF model can be linearised around its operating point to include it in the OPF formulation. This allows for a more efficient computation with almost no loss of accuracy. Especially in real-time control where the states are computed with sub-second time resolution, consecutive states will not vary much. Therefore, linearising

assume that the controllable resources are photovoltaic plants that can curtail their production: $P_i^{pv}, \forall i \in \mathcal{N}^{pv}$.

The objective we minimize at time t is:

$$\min_{P_i^{pv,t}, Q_l^t, E_k^t} (Q_s^t)^2 + \sum_{i \in \mathcal{N}^{pv}} (P_i^{pv,t} - \hat{P}_i^{pv,t})^2 + (P^{losses,t})^2 \quad (12)$$

where the first term Q_s^t minimises the reactive power injected into the upper layer grid (slack bus) and the second term minimises the losses and the PV curtailment. The third term represents the minimisation of the power losses and prevents the reactive power injected/absorbed by the ICs from counteracting each other. This could occur when the voltage SCs at the ICs nodes are very similar because the nodes are e.g. physically located close to each other.

The problem is solved with respect to the constraints:

$$[\mathbf{E}_{min}^{ac}, \mathbf{E}_{min}^{dc}] \leq |\bar{\mathbf{E}}^t| \leq [\mathbf{E}_{max}^{ac}, \mathbf{E}_{max}^{dc}] \quad (13a)$$

$$0 \leq |\bar{\mathbf{I}}^t| \leq [\mathbf{I}_{max}^{ac}, \mathbf{I}_{max}^{dc}] \quad (13b)$$

$$0 \leq P_i^{pv,t} \leq \hat{P}_i^{pv,t} \quad \forall i \in \mathcal{N}^{pv} \quad (13c)$$

$$-\hat{P}_l \leq P_l^t \leq \hat{P}_l, \quad \forall l \in \Gamma_l \quad (13d)$$

$$-\hat{Q}_l \leq Q_l^t \leq \hat{Q}_l, \quad \forall l \in \Gamma_l \quad (13e)$$

$$Q_s^t = \sum_{i \in \mathcal{N} \cap \mathcal{N}_{slack}} Q_i^t + Q^{losses,t} \quad (13f)$$

$$(8), (9), (10) \text{ and } (11) \quad (13g)$$

where (13c) refers to the maximum photovoltaic generation that is computed using a short-term forecast. Constraints (13d) and (13e) refer to the maximum active and reactive power limits of the IC.

D. Real-time Control Architecture

The real-time control architecture is shown in Fig. 2. At each control timestep (every 2s), the state of the grid is provided by the state estimator [19], and the GHI of the next timestep is used to calculate the Maximum Power Point (MPP) of the photovoltaics [20]. Using the updated state estimate, the SCs are computed as described in Section II to represent the grid constraints in the optimisation problem. Next, the optimisation problem, described in (12) and (13), is solved, and the optimal setpoints are sent to the controllable resources.

III. EXPERIMENTAL SETUP

A. Hybrid AC/DC grid

The experimental validation is performed on the hybrid AC/DC grid located at the Distributed Electrical System Laboratory at the EPFL. The hybrid AC/DC microgrid consists of 18 AC nodes, 8 DC nodes and 4 ICs that operate under voltage control mode, that is, the pair $E_{dc} - Q_{ac}$ is controlled. Both grids have a base power of 100 kVA and a base voltage of 400 V_{ac} and 800 V_{dc}. The hybrid grid is connected to the medium voltage AC grid in the GCP at node B01. The topology and parameters of the hybrid network are presented in Fig. 3.

The hybrid AC/DC grid hosts several **distributed resources**. At node B03, a controllable four-quadrant load

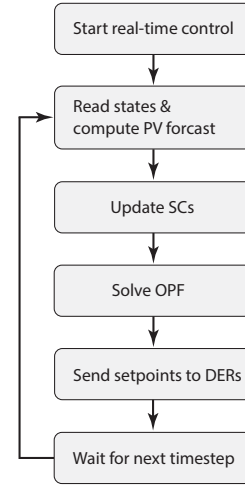


Fig. 2: Flow-chart illustrating the real-time control architecture.

of 30 kVA is connected. The load is operated as a stochastic resource and represents the demand (active and reactive) of a typical household. The node B14 hosts an EVCS with a power rating of 30 kVA that is also modelled as an uncontrollable resource. Three PV plants are connected at node B11. The first plant has a capacity of 13 kVA and is mounted on the facade of a building. The commercial inverter does not allow for curtailment and will always track its MPP. The two other plants have a combined power rating of 16 kVA, and its inverter allows for curtailment.

As shown in Fig. 3, the DC lines are interconnected through **DC/DC converters**. The DC/DC converters are implemented as resonant DC transformers (DCT) and are based on open-loop control [12]. Therefore, they are not controlled through external setpoints, but the power transferred by the DCTs is proportional to the voltage difference between the primary and secondary side. Therefore, by using the IC to optimally regulate the DC voltage, a DC power flow is generated that can be used to redirect power in the AC grid. This linear voltage-power relation is included in the optimisation problem as (14).

$$P_1^{DCT} = \alpha(E_1^{DCT} - E_2^{DCT}) - P_{1,loss} \quad (14a)$$

$$P_2^{DCT} = -\alpha(E_1^{DCT} - E_2^{DCT}) - P_{2,loss} \quad (14b)$$

where 1 refers to the primary and 2 to the secondary side. The coefficient α equals 0.826 kW/V . The two main contributions to the losses P_{loss} are A) the magnetising current required to maintain the magnetising flux in the transformer's core and B) the equivalent ohmic losses of the DCT that are included in the DC grid model as an additional DC line with an equivalent series resistance of 0.46Ω .

It is worth mentioning that this is a simplified model of the DCT. The actual voltage-power profile is not fully linear and includes a zone around $\Delta E = 0$ where the operation is less stable and the power is close to zero. This inaccuracy in the model is the main cause of the uncertainty in the hybrid AC/DC model, as will be shown in Section IV.

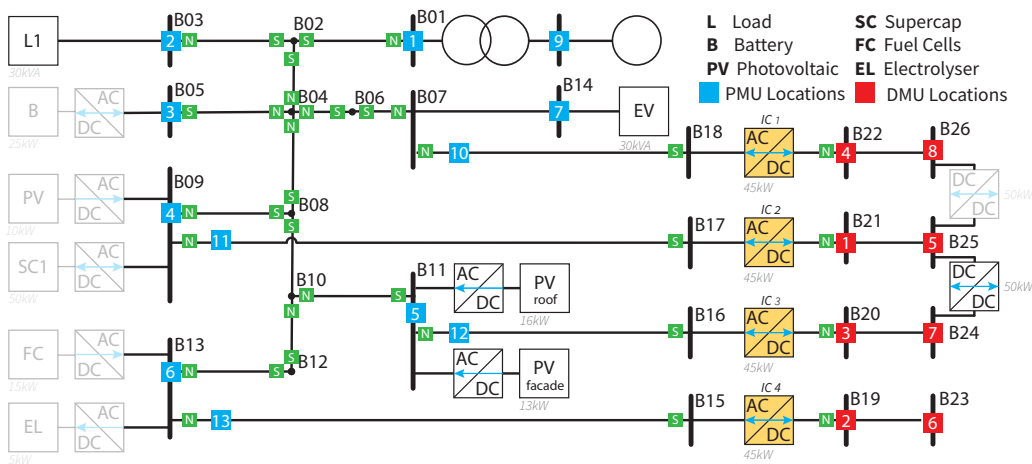


Fig. 3: Hybrid AC/DC microgrid with the connected sources and loads, the maximum power rating is indicated. The table defines the boundary conditions of the simulation.

B. Sensing Infrastructure

The computation of SCs requires knowledge of the nodal voltage at every bus of the hybrid AC/DC grid.

Synchronised measurements are provided every 20 ms by phasor measurement units (PMUs) for the AC grid and DC measurement units (DMUs) on the DC grid. The location of the PMUs and DMU is shown in Figure 3. The PMUs are P-class devices and extract the phasors of measured currents and voltages using an enhanced interpolated discrete Fourier transform (e-IpDFT) [21]. The synchrophasor extraction is time synchronised using GPS and complies with the IEEE standard C37.118 [22] with a total vector error of less than 0.14%. On the DC side, DMUs provide synchronised measurements of DC voltages and current injections. The DMUs use the same procedure as their AC variant, however, the e-IpDFT is replaced by an averaging block. The PMU and DMU measurements are streamed to the phasor data concentrator (PDC) using the user datagram protocol (UDP) [23]. The PDC time aligns the measurements with minimal latency and forwards them to the SE.

The nodal voltage phasors are estimated by the SE and streamed to the real-time control every 100 ms. The SE process for the hybrid AC/DC grid is described in detail in [19]. The method is based on a discrete Kalman filter and uses a unified and linear measurement model of the full hybrid grid, including the ICs. The state variables are typically the nodal voltage phasors. Because of the models' linear nature, the SE is able to compute the most likelihood state using the synchronised AC and DC measurements with subsecond time resolution.

IV. EXPERIMENTAL VALIDATION

The closed-form analytical expression of the SCs is experimentally validated on the hybrid AC/DC microgrid described in Section III. The experiment has been carried out for multiple days. However, in this paper, an interesting case is discussed that was conducted on September 15, 2023, between 15:37 and 16:48. The profiles of the active and reactive power

injection from EVCS, supercapacitor, PV plants (MPP profile) and load emulator, which represents the demand of a typical household, are shown in Figure 4.

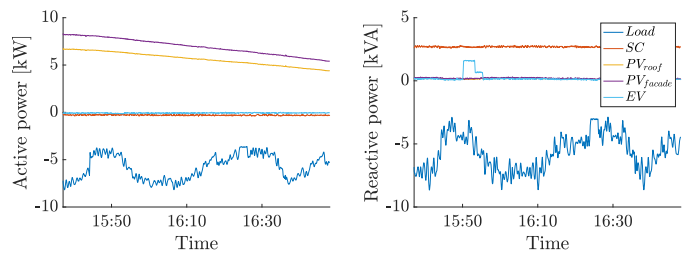


Fig. 4: Active and reactive power of the DER.

In Figure 4, it is shown that the PV generation in node B11 starts decreasing at 15:37 from a cumulative 14.87 kW to 9.82 kW at 16:48. Therefore, the line B10 – B11 will gradually become less congested. The ampacity limits of this line are 15 A, and since we want to minimise the curtailment, a part of the photovoltaic production will be redirected through the DC grid. The branch current of the line B10 – B11 and the ampacity limit are shown in Figure (5). We can observe

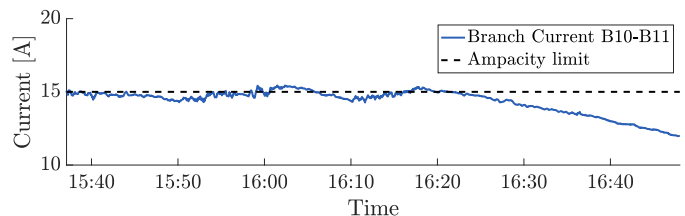


Fig. 5: Current through line B10 – B11 and its ampacity limit.

that the branch current slightly exceeds the ampacity limit in certain instances. The overshoot is never larger than 0.35 A, corresponding to 250 W. This is mainly due to the inaccuracy in the simplified DCT model, as already discussed in Section III. The actual model deviates from a linear power-voltage relation for very small and very large powers. In further research, the DCT model will be better characterised and

included in the real-time controller. The optimal real-time control regulates the DC voltage of IC 2 and IC 3 to create a power flow through the DCT to avoid curtailment. The power through the DCT is shown in Figure 6 (left). After 16:20, PV production no longer exceeds the line ampacity limit, and DCT stops transferring power. We also see that the power of the DCT does not go to zero after this time but reaches around -600 W. This is due to the transformer losses that are equally allocated to its primary and secondary side.

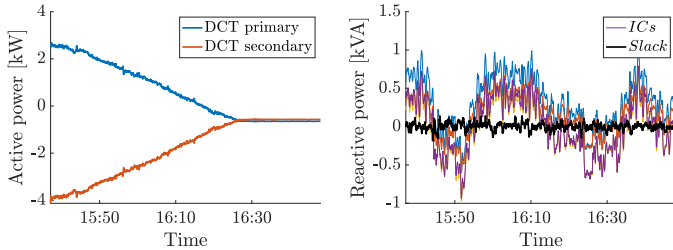


Fig. 6: Active and reactive power of the controllable resources i.e., the ICs and DCT

Additionally, the objective of real-time control aims at minimising the reactive power at the GCP. In Figure 6 (right), the reactive power that is injected by the ICs is shown to minimise the reactive power at the slack node. We can see that the reactive power at the slack (in black) is very close to zero. Due to the loss term that is added to the objective in (12), the ICs only inject a minimal reactive power and do not counteract each other.

A. Validation of the SC-based grid model

The accuracy of the grid model, which is represented by the SCs, is shown in Figure 7. The accuracy metric is defined as the difference between the actual grid voltage and the grid voltage that was expected by the control action. The mean of the voltage error of all the nodes is indicated in dark blue. The shaded light blue area represents the minimum and maximum voltage error at each timestep. We see that the voltage error is very small with an average of -7.62×10^{-5} over the experiment. Therefore, the SC-based grid model is valid.

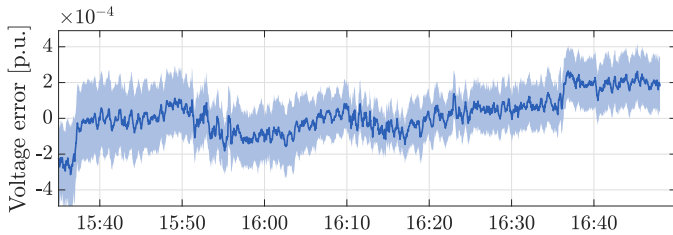


Fig. 7: Voltage error of the SC-based model

B. Computational time analysis

The computational time of the real-time controller is evaluated and shown as a cumulative distribution function in Figure 8. The CPU time includes the time of the full control process presented in Figure 2, that is, fetching the grid state and GHI, computing the SC, solving the optimisation problem,

and sending the setpoints to the resources. The overall time has an upper limit of 1.5 s and is therefore very well suitable for critical real-time control processes.

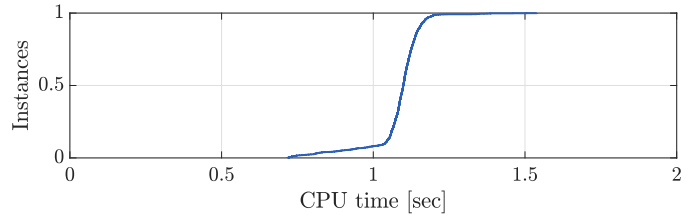


Fig. 8: Cumulative distribution function of the computational time of the full real-time control.

V. CONCLUSION

In this paper, we present the experimental validation of a grid-aware optimal control of hybrid AC/DC microgrids leveraged by the closed-form computation of the voltage SCs. The analytical computation of the SC for hybrid AC/DC grids is presented in the author's previous work and is based on a unified PF model that accounts for the AC grid, DC grid, and the various operation modes of the ICs.

The optimal SC-based control is validated on the hybrid AC/DC microgrid available at the EPFL. The microgrid consists of 18 AC nodes, 8 DC nodes, and 4 ICs. PMUs and DMUs provide synchronised AC and DC measurements to a linear SE that estimates the state of the network every 100 ms. The state is streamed to the real-time control to update the SCs at every timestep.

In a use case, it is shown that the real-time control operates correctly and avoids the need for PV curtailment by redirecting power through the DC grid to relax a congested AC line. The error in the SC-based model is on the order of 10^{-5} for the nodal voltages of both the AC and DC networks. Furthermore, it is shown that the full real-time control process (this includes reading the states, computing the SC, solving the OPF, and sending the updated resources setpoints) takes less than 1.5 s. Therefore, it is very well applicable for the real-time control of hybrid AC/DC networks.

APPENDIX

The voltage SC are computed as follows:

- 1) Compute the partial derivative of the PF equations (presented in [13]) to \mathcal{X} , shown in (15).
- 2) Regroup the partial derivatives in the form $\mathbf{Ax}(\mathcal{X}) = \mathbf{u}(\mathcal{X})$, where $\mathbf{x}(\mathcal{X})$ are the voltage sensitivity coefficients $\frac{\partial \bar{E}}{\partial \mathcal{X}}$ as described in (3).
- 3) Solve the linear system of equations.

To simplify the expressions of the partial derivative, two new variables are introduced $\bar{F}_{i,n}^{ac} = \bar{E}_i \underline{Y}_{i,n}^{ac} \underline{E}_n$ and $F_{j,m}^{dc} = E_j Y_{j,m}^{dc} E_m$.

AC nodes :

$$\sum_{n \in \mathcal{N}} \Re\{\bar{F}_{i,n}^{ac}\} \left[\frac{1}{|\bar{E}_i|} \frac{\partial |\bar{E}_i|}{\partial \mathcal{X}} + \frac{1}{|\bar{E}_n|} \frac{\partial |\bar{E}_n|}{\partial \mathcal{X}} \right] - \sum_{n \in \mathcal{N}} \Im\{\bar{F}_{i,n}^{ac}\} \left[\frac{\partial \angle \bar{E}_i}{\partial \mathcal{X}} - \frac{\partial \angle \bar{E}_n}{\partial \mathcal{X}} \right] = \frac{\partial P_i^{\phi*}}{\partial \mathcal{X}}, \quad \forall i \in \mathcal{N}_{PQ} \cup \mathcal{N}_{PV} \quad (15a)$$

$$\sum_{n \in \mathcal{N}} \Im\{\bar{F}_{i,n}^{ac}\} \left[\frac{1}{|\bar{E}_i|} \frac{\partial |\bar{E}_i|}{\partial \mathcal{X}} + \frac{1}{|\bar{E}_n|} \frac{\partial |\bar{E}_n|}{\partial \mathcal{X}} \right] + \sum_{n \in \mathcal{N}} \Re\{\bar{F}_{i,n}^{ac}\} \left[\frac{\partial \angle \bar{E}_i}{\partial \mathcal{X}} - \frac{\partial \angle \bar{E}_n}{\partial \mathcal{X}} \right] = \frac{\partial Q_i^{\phi*}}{\partial \mathcal{X}}, \quad \forall i \in \mathcal{N}_{PQ} \quad (15b)$$

$$\frac{\partial \bar{E}_i}{\partial \mathcal{X}} = \frac{\partial \bar{E}_i^{\phi*}}{\partial \mathcal{X}}, \quad \forall i \in \mathcal{N}_{PV} \quad (15c)$$

DC nodes :

$$\sum_{m \in \mathcal{M}} F_{j,m}^{dc} \left[\frac{1}{E_j} \frac{\partial E_j}{\partial \mathcal{X}} + \frac{1}{E_m} \frac{\partial E_m}{\partial \mathcal{X}} \right] = \frac{\partial P_j^*}{\partial \mathcal{X}}, \quad \forall j \in \mathcal{M}_P \quad (15d)$$

$$\frac{\partial E_j}{\partial \mathcal{X}} = \frac{\partial E_j^*}{\partial \mathcal{X}}, \quad \forall j \in \mathcal{M}_V \quad (15e)$$

IC nodes :

$$\sum_{n \in \mathcal{N}} \Re\{\bar{F}_{i,n}^{ac}\} \left[\frac{1}{|\bar{E}_i|} \frac{\partial |\bar{E}_i|}{\partial \mathcal{X}} + \frac{1}{|\bar{E}_n|} \frac{\partial |\bar{E}_n|}{\partial \mathcal{X}} \right] - \sum_{n \in \mathcal{N}} \Im\{\bar{F}_{i,n}^{ac}\} \left[\frac{\partial \angle \bar{E}_i}{\partial \mathcal{X}} - \frac{\partial \angle \bar{E}_n}{\partial \mathcal{X}} \right] - \frac{\partial P_{(l,k)}^{loss}}{\partial \mathcal{X}} = \frac{\partial P_l^*}{\partial \mathcal{X}}, \quad \forall l \in \Gamma_{PQ} \quad (15f)$$

$$\sum_{n \in \mathcal{N}} \Im\{\bar{F}_{i,n}^{ac}\} \left[\frac{1}{|\bar{E}_i|} \frac{\partial |\bar{E}_i|}{\partial \mathcal{X}} + \frac{1}{|\bar{E}_n|} \frac{\partial |\bar{E}_n|}{\partial \mathcal{X}} \right] + \sum_{n \in \mathcal{N}} \Re\{\bar{F}_{i,n}^{ac}\} \left[\frac{\partial \angle \bar{E}_i}{\partial \mathcal{X}} - \frac{\partial \angle \bar{E}_n}{\partial \mathcal{X}} \right] - \frac{\partial Q_{(l,k)}^{loss}}{\partial \mathcal{X}} = \frac{\partial Q_l^*}{\partial \mathcal{X}}, \quad \forall l \in \Gamma_{PQ} \cup \Gamma_{VdcQ} \quad (15g)$$

$$\sum_{n \in \mathcal{N}} \Re\{\bar{F}_{l,n}^{ac}\} \left[\frac{1}{|\bar{E}_l|} \frac{\partial |\bar{E}_l|}{\partial \mathcal{X}} + \frac{1}{|\bar{E}_n|} \frac{\partial |\bar{E}_n|}{\partial \mathcal{X}} \right] - \sum_{n \in \mathcal{N}} \Im\{\bar{F}_{l,n}^{ac}\} \left[\frac{\partial \angle \bar{E}_l}{\partial \mathcal{X}} - \frac{\partial \angle \bar{E}_n}{\partial \mathcal{X}} \right] + \frac{\partial P_{(l,k)}^{filter}}{\partial \mathcal{X}} + \frac{\partial P_{(l,k)}^{loss}}{\partial \mathcal{X}} = \sum_{m \in \mathcal{M}} F_{k,m}^{dc} \left[\frac{1}{E_k^*} \frac{\partial E_k^*}{\partial \mathcal{X}} + \frac{1}{E_m} \frac{\partial E_m}{\partial \mathcal{X}} \right], \quad \forall (l,k) \in \Gamma_{VdcQ} \quad (15h)$$

- [1] N. Eghtedarpour and E. Farjah, "Power control and management in a hybrid ac/dc microgrid," *IEEE transactions on smart grid*, vol. 5, no. 3, pp. 1494–1505, 2014.
- [2] Y. R. Li, F. Nejbatkhan, and H. Tian, *Smart Hybrid AC/DC Microgrids*. Wiley-IET Press, 2023, pp. 1–20.
- [3] Z. Yang, H. Zhong, A. Bose, Q. Xia, and C. Kang, "Optimal power flow in ac–dc grids with discrete control devices," *IEEE Transactions on Power Systems*, vol. 33, no. 2, pp. 1461–1472, 2017.
- [4] M. Hotz and W. Utschick, "hynet: An optimal power flow framework for hybrid ac/dc power systems," *IEEE Transactions on Power Systems*, vol. 35, no. 2, pp. 1036–1047, 2019.
- [5] A. Eajal *et al.*, "A unified approach to the power flow analysis of ac/dc hybrid microgrids," *IEEE Transactions on sustainable energy*, vol. 7, no. 3, pp. 1145–1158, 2016.
- [6] A. Mešanović, U. Muenz, and C. Ebenbauer, "Robust optimal power flow for mixed ac/dc transmission systems with volatile renewables," *IEEE Transactions on Power Systems*, vol. 33, no. 5, pp. 5171–5182, 2018.
- [7] N. Qachchachi, H. Mahmoudi, and A. El Hasnaoui, "Optimal power flow for a hybrid ac/dc microgrid," in *2014 International Renewable and Sustainable Energy Conference (IRSEC)*. IEEE, 2014, pp. 559–564.
- [8] M. Hosseinzadeh and F. R. Salmasi, "Robust optimal power management system for a hybrid ac/dc micro-grid," *IEEE Transactions on Sustainable Energy*, vol. 6, no. 3, pp. 675–687, 2015.
- [9] M. Baradar, M. R. Hesamzadeh, and M. Ghandhari, "Second-order cone programming for optimal power flow in vsc-type ac-dc grids," *IEEE Transactions on Power Systems*, vol. 28, no. 4, pp. 4282–4291, 2013.
- [10] J. Li, F. Liu, Z. Wang, S. H. Low, and S. Mei, "Optimal power flow in stand-alone dc microgrids," *IEEE Transactions on Power Systems*, vol. 33, no. 5, pp. 5496–5506, 2018.
- [11] A. Alvarez-Bustos, B. Kazemtabrzi, M. Shahbazi, and E. Acha-Daza, "Universal branch model for the solution of optimal power flows in hybrid ac/dc grids," *International Journal of Electrical Power & Energy Systems*, vol. 126, p. 106543, 2021.
- [12] R. P. Barcelos and D. Dujčić, "Direct current transformer impact on the dc power distribution networks," *IEEE Transactions on Smart Grid*, vol. 13, no. 4, pp. 2547–2556, 2022.
- [13] W. Lambrichts and M. Paolone, "General and unified model of the power flow problem in multiterminal ac/dc networks," *submitted to IEEE Transactions on Power Systems*, 2023, publisher: arXiv.
- [14] K. Christakou, "Real-time optimal controls for active distribution networks: from concepts to applications," *European Journal of Organic Chemistry*, vol. 2012, pp. 7112–7119, 2015.
- [15] W. Lambrichts and M. Paolone, "Analytically computation of sensitivity coefficients in hybrid ac/dc micro-grid," *submitted to IEEE transactions on smart grids*, under review, 2023, publisher: arXiv.
- [16] —, "Linear recursive state estimation of hybrid and unbalanced ac/dc micro-grids using synchronized measurements," *IEEE Transactions on Smart Grid*, 2022.
- [17] M. Baradar, M. Ghandhari, and D. Van Hertem, "The modeling multi-terminal vsc-hvdc in power flow calculation using unified methodology," in *2011 2nd IEEE ISGT*. IEEE, 2011, pp. 1–6.
- [18] W. Lambrichts and M. Paolone, "Hybrid-AC-DC-grid," 4 2023. [Online]. Available: <https://github.com/DESL-EPFL/Hybrid-AC-DC-grid>
- [19] —, "Experimental validation of a unified and linear state estimation method for hybrid ac/dc microgrids," in *2023 IEEE Belgrade PowerTech*. IEEE, 2023, pp. 1–8.
- [20] R. Gupta, F. Sossan, and M. Paolone, "Grid-aware distributed model predictive control of heterogeneous resources in a distribution network: Theory and experimental validation," *IEEE Transactions on Energy Conversion*, vol. 36, no. 2, pp. 1392–1402, 2020.
- [21] P. Romano and M. Paolone, "Enhanced interpolated-dft for synchrophasor estimation in fpgas: Theory, implementation, and validation of a pmu prototype," *IEEE Transactions on instrumentation and measurement*, vol. 63, no. 12, pp. 2824–2836, 2014.
- [22] "Ieee standard for synchrophasor measurements for power systems," *IEEE Std C37.118.1-2011*, pp. 1–61, 2011.
- [23] A. Derviškić, P. Romano, M. Pignati, and M. Paolone, "Architecture and experimental validation of a low-latency phasor data concentrator," *IEEE Transactions on Smart Grid*, vol. 9, no. 4, pp. 2885–2893, 2018.